

Quantum echo dynamics in the Sherrington-Kirkpatrick model

Silvia Pappalardi ^{1,2,3,*}, Anatoli Polkovnikov ³ and Alessandro Silva ²

1 SISSA — International School for Advanced Studies, via Bonomea 265, I-34136 Trieste, Italy

2 Abdus Salam ICTP — International Center for Theoretical Physics, Strada Costiera 11, I-34151 Trieste, Italy

3 Department of Physics, Boston University, 590 Commonwealth Avenue, Boston, Massachusetts 02215, USA

* spappala@sissa.it

June 10, 2022

Abstract

Understanding the footprints of chaos in quantum-many-body systems has been under debate for a long time. In this work, we study the echo dynamics of the Sherrington-Kirkpatrick (SK) model with transverse field under effective time reversal. We investigate numerically its quantum and semiclassical dynamics. We explore how chaotic many-body quantum physics can lead to exponential divergence of the echo of observables and we show that it is a result of three requirements: i) the collective nature of the observable, ii) a properly chosen initial state and iii) the existence of a well-defined semi-classical (large- N) limit. Under these conditions, the echo grows exponentially up to the Ehrenfest time, which scales logarithmically with the number of spins N . In this regime, the echo is well described by the semiclassical (truncated Wigner) approximation. We also discuss a short-range version of the SK model, where the Ehrenfest time does not depend on N and the quantum echo shows only polynomial growth. Our findings provide new insights on scrambling and echo dynamics and how to observe it experimentally.

Contents

1	Introduction	2
2	Echo dynamics and scrambling	4
3	The choice of the initial state and the observable	5
3.1	Early-time growth	5
3.2	Long time saturation	6
3.3	Existence of a parametric window for the echo growth	8
4	The Sherrington-Kirkpatrick model in transverse field	9

5	Truncated Wigner Approximation (TWA) in the large N-limit	10
5.1	TWA for the SK model	11
5.2	TWA for the short-range model	13
6	Scrambling in the SK model	14
6.1	Absence of exponential sensitivity with short-range interactions	17
7	Discussion	19
A	Echo dynamics for the magnetization along y	19
	References	21

1 Introduction

Understanding how irreversibility arises in classical and quantum systems has been of pivotal importance since the foundations of statistical mechanics [1–4]. One of the most widely used ways to characterise chaotic dynamics in the quantum domain is the study of imperfect time-reversal evolution of the wave function, in particular, the *Loschmidt echo* [4]. Under classical chaotic dynamics, as a result of the exponential sensitivity of trajectories to small perturbations, any imperfection in a time-reversed protocol hinders a full recovery of the initial information, making time-reversal impossible in practice. Analogous approaches have been explored successfully in few-body quantum systems [5–7] but, as far as many-body systems are concerned, the onset of chaos is still the focus of an intense debate [8–10].

The topic was recently revived with a new name: *scrambling* [11–16]. This revival was mostly motivated by Kitaev’s proposal to quantify chaos in many-body systems in terms of the growth in time of the square the non-equal time commutator of two initially commuting observables [13], or of the closely connected out of time order correlators (OTOC). In fact, these quantities are connected in the semi-classical limit to the Lyapunov instabilities of classical trajectories [14–16].

Much before scrambling, these questions were addressed in the context of *nuclear magnetic resonance* (NMR) “magic echo” experiments [17–20], where irreversibility is characterized via the macroscopic response of some physical observable under imperfect time-reversal. A first attempt to analyze chaos of many-body quantum systems through the echo was made by B. Fine and collaborators in Refs. [21] and [22] for particular spins systems. There, it was found that the exponential sensitivity of the echo only applies to quantum systems close to their classical limit. More recently, it has been understood that the echo of observables is intimately linked to the square commutator and to OTOC, see also Refs. [23–26] for related developments.

In the classical limit, the square of a non-equal time commutator of two observables maps to the square of the non-equal time Poisson bracket of the corresponding classical functions [14–16]. Thus, the expectation value of the square commutator over the initial quantum state corresponds to the averaging of the corresponding square Poisson bracket over the ini-

tial probability distribution, e.g. given by the Wigner function. Therefore, one anticipates that at least near the classical limit the square commutator should grow exponentially fast in time with a rate given by the maximal Lyapunov exponent (similar considerations apply to the echo). Indeed examples of quantum exponential sensitivity have been found only in models of few-particle systems near well-defined semi-classical limits [27–31] and in the large- N limit of a Sachdev-Ye-Kitaev (SYK) model, a solvable model of all-to-all interacting fermions [13, 26, 32]. On the other hand, following the initial observation of Ref. [21] it was proven that for spin or fermionic systems with local interactions the OTOC of local observables or sums of local observables grows at most polynomially in time [33]. However, to date, the mechanisms that underpin the above footprints of chaos in many-body quantum systems are not fully understood.

In this work, we investigate how chaotic many-body quantum dynamics leads to exponential divergence of the echo observables in the transverse Sherrington-Kirkpatrick (SK) spin model with long-range interactions. This model has many analogies with the SYK model and serves as a paradigmatic example of quantum glasses [34–36]. Interestingly, its Hamiltonian can be experimentally realised over different atomic platforms ranging from cavity QED to Rydberg atoms, where it has been proposed as a way to access scrambling via interferometry [37]. Because of disordered couplings, there is no natural classical limit in this model, in a way similar to the SYK model. Yet we show that the semiclassical truncated Wigner approximation (TWA) [38–41] can accurately reproduce the echo up to the Ehrenfest time provided the observable and the initial state are chosen correctly. In this sense, the large N limit of this model is semiclassical, like for the SYK model [26]. We also find that the nature of the initial state and of the observable are crucial to observe exponential echo response in this and other large N models. In order to emphasize the role of a well-defined semi-classical limit, we also consider a short-range version of the SK model, with random couplings between sites decaying gaussianly as a function of their distance. In this case, the semi-classical description fails to correctly reproduce the echo dynamics, which do not show any exponential sensitivity to the protocol time.

In order to see exponential growth of the OTOC, the operator and the initial state have to be such that there is a “long” time window (divergent in the thermodynamic limit) between the early time power-law growth and the late time saturation. In loose terms, the operator on the initial state has to give enough “space” to the OTOC to develop the exponential growth. This is clearly impossible in quantum systems with a bounded local Hilbert space size like in spin 1/2 chains or Hubbard like models of interacting fermions if we choose local in space observables. Such operators are bounded by the corresponding finite operator norms at long times and generically do not give room for exponential growth. In Ref. [33] it was thus argued that collective observables such as the sums of local observables, which can become arbitrarily large with the number of degrees of freedom, are better candidates for observing universal, non-perturbative behavior of OTOC. Thus, given a collective observable, one has to require that the long-time saturation value of the OTOC has a parametrically larger value in the system size N than the coefficient governing the initial perturbative short-time behaviour. Interestingly, such requirements simultaneously constrain the nature of the initial state and of the observable. In particular, we find that for a collective observable the “good” initial state must be such that there is an extensive difference between the initial and the equilibrium (long time) values of the observable. For example, if we choose total (non-conserved) magnetization as an observable, which decays to zero under forward evolution, one could

start from an initially magnetized state. In the case of a current as an observable, a good initial state will be the one with a macroscopic current, and so on.

Such initial states naturally generalize those proposed by Rozenbaum et al. in Ref. [42], where the authors associated the existence of an exponential regime with the choice of the “classical” initial conditions localized in phase space, where the position and the momentum of the particle acquire non-zero expectation values. This choice of initial conditions is very similar to that proposed in Ref. [21] for studying the echo based on more intuitive considerations. As in recent studies of the SYK model, we find that in order to observe exponential behavior of the OTOC it is necessary to have long-range interactions in the system, correctly captured by semiclassical TWA dynamics. In this way, even in the absence of an obvious classical limit in the system, $1/N$ serves as an effective Planck’s constant \hbar . Note that, because of the disorder, the SK model can not be mapped onto a large spin model, and thus the classical behavior of the model in the large N -limit is not self-evident. Our work therefore confirms the existence of quantum Lyapunov exponents is closely related to the proximity of the model to the semiclassical limit, coinciding with the corresponding classical exponents [27–31] (c.f. Ref. [26] for the SYK model). Notice that in Ref. [32] it was argued that classical Lyapunov exponents can exceed the quantum one in SYK model. However, the authors of the paper considered initial conditions sampled according to the classical thermal Gibbs distribution rather than the corresponding Wigner function. The two choices can lead to inconsistencies between the conclusions, since the exponential growth crucially depends on the initial state.

The rest of the paper is organized as follows. In Section 2 we introduce the echo operator and discuss the connection between echo dynamics and scrambling. In Section 3 we discuss the requirements on the initial state and the observables. Then, in Section 4 we describe the Sherrington-Kirkpatrick (SK) model and its short-range version. In the following Section 5, we summarize the main aspects of the TWA and show its validity for the SK model in the thermodynamic limit and its failure for the short-range case. Finally in Section 6, we show numerical results and determine the Lyapunov exponent for the long-range model.

2 Echo dynamics and scrambling

Let us start with a description of the protocol we are studying: an imperfect time reversal through the echo response of an observable, in a spirit similar to Loschmidt echo experiments and to NMR magic echoes (see Refs. [21] and [26]). In this setting, the system is prepared in a polarized state of some observable \hat{A} , such as the magnetization in some direction, and it is then allowed to evolve under the action of the Hamiltonian \hat{H} for a certain time t . At time t , it is then subject to a rapid rotation generated by the unitary operator $e^{i\epsilon\hat{B}}$ and then it evolves back under the reversed Hamiltonian $-\hat{H}$ for an identical time interval t . Afterwards, the observable \hat{A} is measured. The corresponding time-evolved operator \hat{A}_ϵ reads: [26]

$$\begin{aligned}\hat{A}_\epsilon(t) &= e^{-i\hat{H}t} e^{-i\epsilon\hat{B}} e^{i\hat{H}t} \hat{A} e^{-i\hat{H}t} e^{i\epsilon\hat{B}} e^{i\hat{H}t} = e^{-i\epsilon\hat{B}(t)} \hat{A} e^{i\epsilon\hat{B}(t)} \\ &= \hat{A} - i\epsilon [\hat{B}(t), \hat{A}] - \frac{\epsilon^2}{2} [\hat{B}(t), [\hat{B}(t), \hat{A}]] + \mathcal{O}(\epsilon^3),\end{aligned}\tag{1}$$

where $\hat{B}(t) = e^{-i\hat{H}t} \hat{B} e^{i\hat{H}t}$ is the perturbing operator in the Heisenberg representation with respect to the forward Hamiltonian \hat{H} .

The expectation value of the difference $\hat{A}_\epsilon(t) - \hat{A}$ on a generic quantum state $|\psi_0\rangle$ corresponds to the *observable's echo response*. The term proportional to ϵ appears in a standard Kubo-type linear response susceptibility. It does not contain any information about OTOC and in general should be subtracted from the echo. If the initial state $|\psi_0\rangle$ is an eigenstate of \hat{A} , then this term vanishes and the leading order term of the difference is the second one [26], proportional to an OTOC. From now on we will deal only with such states. It is thus useful to define $\mu(t)$, characterizing the echo, as

$$\mu(t) = \lim_{\epsilon \rightarrow 0} \frac{1}{\epsilon^2} \langle \hat{A}_\epsilon(t) - \hat{A} \rangle_0 = -\frac{1}{2} \langle [\hat{B}(t), [\hat{B}(t), \hat{A}]] \rangle_0, \quad (2)$$

where $\langle \dots \rangle_0$ stands for the average with respect to the initial state. The function $\mu(t)$ describes the sensitivity of the dynamics to small perturbations. It contains OTOC and in the classical limit is proportional to the square of the Poisson bracket of $\hat{B}(t)$ and \hat{A} thus exponentially diverging with twice the Lyapunov exponent (c.f. Refs. [5, 21, 26]). Interestingly, *the square commutator* $-\langle [\hat{B}(t), \hat{A}]^2 \rangle$ [13–16, 27–30, 32], in this language corresponds to the second moment of $\hat{A}_\epsilon(t) - \hat{A}$ computed with Eq.(1) at second order in ϵ (see Ref. [43, 44] for a related discussion). This connection clarifies in what sense the concepts of scrambling and echo dynamics are related. For this reason, we will use the two notions interchangeably for the rest of the paper. A very interesting and open question concerns the distribution of the echo operator $\hat{A}_\epsilon(t) - \hat{A}$. We will leave this study for future work and focus here only on studying its expectation value $\mu(t)$.

3 The choice of the initial state and the observable

In this section, we discuss the conditions for the existence of a long time-window that provides enough “room” for exponential growth, connected to chaos, to develop. This amounts to requiring that the long-time saturation value of the echo is parametrically larger in the system size N than the coefficient governing its initial perturbative short-time expansion. Let us explain this point, first analyzing the short-time regime with perturbation theory and then the long-time saturation value, evaluated with the Eigenstate Thermalization Hypothesis (ETH) [45, 46]. We will show in the generic case of a sufficiently chaotic spin Hamiltonian satisfying ETH, that the condition above is met if one chooses i) either the perturbation \hat{B} or the observable \hat{A} to be collective (sum of local operators), ii) the initial expectation value of \hat{A} in the state $|\psi_0\rangle$ far from the long-time (thermal) saturation value. As we already mentioned above, while it is not required the analysis significantly simplifies if the initial state is the eigenstate of \hat{A}

$$|\psi_0\rangle = |\alpha_0\rangle \quad : \quad \hat{A}|\alpha_0\rangle = \alpha_0 |\alpha_0\rangle. \quad (3)$$

3.1 Early-time growth

We will therefore assume this condition to be met. Using Eq.(3), the average of the echo operator in Eq.(2) becomes

$$\mu(t) = \langle \hat{B}(t) \hat{A} \hat{B}(t) \rangle - \alpha_0 \langle \hat{B}^2(t) \rangle. \quad (4)$$

In order to derive the early-time behaviour, it is more convenient to work in the eigenbasis of the operator \hat{A} , i.e. $\hat{A}|\alpha_\lambda\rangle = \alpha_\lambda |\alpha_\lambda\rangle$ with $\lambda = 0, \dots, D-1$, where D is the Hilbert space

dimension ($D = 2^N$ for a system of N spin $1/2$). The early-time expansion of the operator $\hat{B}(t)$ can be obtained via the Baker–Campbell–Hausdorff formula. Up to second order in time it reads

$$\hat{B}(t) = \hat{B} - it[\hat{H}, \hat{B}] - t^2/2[\hat{H}, [\hat{H}, \hat{B}]] + \mathcal{O}(t^3) . \quad (5)$$

We will further assume that the operators \hat{A} and \hat{B} commute at $t = 0$. This guarantees that $\mu(0) = 0$, i.e. that the echo signal in \hat{A} only appears after some propagation time. For this reason the operators \hat{A} and \hat{B} can be simultaneously diagonalized such that $\hat{B}|\alpha_\lambda\rangle = \beta_\lambda|\alpha_\lambda\rangle$. At short times, the average of the echo operator (4) reads

$$\mu(t) = t^2 \sum_{\lambda \neq 0} |\hat{H}_{0\lambda}|^2 (\beta_i - \beta_0)^2 (\alpha_\lambda - \alpha_0) + \mathcal{O}(t^4) , \quad (6)$$

where $|\hat{H}_{0\lambda}| = \langle \alpha_0 | \hat{H} | \alpha_\lambda \rangle$ are the matrix elements of Hamiltonian matrix elements in the eigenbasis of \hat{A} .

3.2 Long time saturation

Let us now turn to the analysis of the long time saturation of the echo, or more precisely of the infinite time average of Eq.(2)

$$\bar{\mu} = \lim_{T \rightarrow \infty} \frac{1}{T} \int_0^T \mu(t) dt .$$

Now it is convenient to work in the eigenbasis of the Hamiltonian, i.e. $\hat{H} |E_n\rangle = E_n |E_n\rangle$. Then Eq. (4) can be re-written as

$$\mu(t) = \sum_{nmpq} c_n c_q^* B_{nm} A_{mp} B_{pq} e^{i(E_n - E_m + E_p - E_q)t} - \alpha_0 \sum_{nmp} c_n c_m^* B_{np} B_{pm} e^{i(E_n - E_m)t} , \quad (7)$$

where $c_n = \langle \psi_0 | E_n \rangle$, $B_{nm} = \langle E_n | \hat{B} | E_m \rangle$ and $A_{nm} = \langle E_n | \hat{A} | E_m \rangle$. We will assume that the Hamiltonian \hat{H} is chaotic satisfying ETH and in particular that it has no degeneracies. With this choice, the time average of Eq.(7) is non-zero only if the energies appearing in the exponentials are equal to each other pairwise, [45, 46] such that

$$\overline{e^{i(E_n - E_m + E_p - E_q)t}} = \delta_{nm} \delta_{pq} + \delta_{nq} \delta_{mp} - \delta_{nmpq} ,$$

where δ_{nmpq} implies that all four indices are equal to each other. Likewise

$$\overline{e^{i(E_n - E_m)t}} = \delta_{nm} .$$

Then

$$\begin{aligned} \bar{\mu} &= \sum_{nm} c_n c_m^* B_{nn} A_{nm} B_{mm} + \sum_{nm} |c_n|^2 |B_{nm}|^2 A_{mm} - \sum_n |c_n|^2 B_{nn}^2 A_{nn} - \alpha_0 \sum_{nm} |c_n|^2 |B_{nm}|^2 \\ &= \sum_{nm} c_n c_m^* B_{nn} A_{nm} B_{mm} - \alpha_0 \sum_n |c_n|^2 |B_{nn}|^2 + \sum_{n \neq m} |c_n|^2 (A_{mm} - \alpha_0) |B_{nm}|^2 . \end{aligned} \quad (8)$$

This expression further simplifies if we assume that the diagonal matrix elements B_{nn} are smooth functions of E_n , an assumption always justified within ETH. If indeed the energy

fluctuations of the initial state $\delta^2 E = \langle \psi_0 | \hat{H}^2 | \psi_0 \rangle - \langle \psi_0 | \hat{H} | \psi_0 \rangle^2$ are sub-extensive $\delta E^2 / E^2 \sim 1/N$ [46], owing to the fact that $\sum_{nm} c_n c_m^* A_{nm} = \alpha_0$ and $\sum |c_n|^2 = 1$, the first two terms in the expression above cancel each other and we get

$$\bar{\mu} \approx \sum_{n \neq m} |c_n|^2 (A_{mm} - \alpha_0) |B_{nm}|^2. \quad (9)$$

We can now compute the long-time saturation value using the ETH ansatz for the matrix elements of observables in the eigenbasis of the Hamiltonian. The latter is formally stated as [45, 46]

$$A_{nm} = \mathcal{A}(\bar{E}) \delta_{nm} + e^{-S(\bar{E})/2} f_{\hat{A}}(\bar{E}, \omega) R_{nm}, \quad (10)$$

where $\bar{E} = (E_n + E_m)/2$, $\omega = E_m - E_n$, $S(\bar{E})$ is the micro-canonical entropy and R_{nm} is a random variable with zero average and unit variance. Both $\mathcal{A}(\bar{E})$ and $f_{\hat{A}}(\bar{E}, \omega)$ are smooth functions of their arguments. We can now substitute it into E.(9) and obtain

$$\bar{\mu} = \sum_{n \neq m} |c_n|^2 [\mathcal{A}(E_n + \omega) - \alpha_0] |f_{\hat{B}}(E_n + \omega/2, \omega)|^2 e^{-S(E_n + \omega/2)}. \quad (11)$$

where we have replaced R_{mm} ($|R_{nm}|^2$) with its statistical zero (unit) average and $\bar{E} = E_n + \omega/2$ and $E_m = E_n + \omega$. We now write each sum as an integral with the suitable density of states, $\sum_m \rightarrow \int_0^\infty dE_m e^{S(E_m)} = \int d\omega e^{S(E+\omega)}$. We therefore have

$$\bar{\mu} = \sum_n |c_n|^2 \int d\omega [\mathcal{A}(E_n + \omega) - \alpha_0] |f_{\hat{B}}(E_n + \omega/2, \omega)|^2 e^{-S(E_n + \omega/2) + S(E_n + \omega)}. \quad (12)$$

Since $f_{\hat{B}}(E, \omega)$ decays rapidly enough at large ω [47], we can expand in powers of ω

$$\mathcal{A}(E_n + \omega) = \mathcal{A}(E) + \frac{\partial \mathcal{A}}{\partial E} \omega + \dots \quad (13a)$$

Notice that if \hat{A} is a local operator, or a sum of local operators, the term containing the energy derivative become irrelevant in the thermodynamic limit [46]. Substituting back, we obtain

$$\begin{aligned} \bar{\mu} &= \sum_n |c_n|^2 [\mathcal{A}(E_n) - \alpha_0] \int d\omega |f_{\hat{B}}(E_n + \omega/2, \omega)|^2 e^{-S(E_n + \omega/2) + S(E_n + \omega)} \\ &= \sum_n |c_n|^2 [\mathcal{A}(E_n) - \alpha_0] \langle E_n | \Delta \hat{B}^2 | E_n \rangle \end{aligned} \quad (14)$$

where we have replaced the frequency integral by the variance over a single energy eigenstate $\langle E_n | \Delta \hat{B}^2 | E_n \rangle = \langle E_n | \hat{B}^2 | E_n \rangle - \langle E_n | \hat{B} | E_n \rangle^2$, see Ref. [46]. Performing now an expansion around the average energy $E = \langle \psi_0 | \hat{H} | \psi_0 \rangle$

$$\mathcal{A}(E_n) = \mathcal{A}(E) + (E_n - E) \mathcal{A}'(E) + \frac{1}{2} (E_n - E)^2 \mathcal{A}''(E) + \dots \quad (15)$$

where $\mathcal{A}'(E) = \frac{\partial \mathcal{A}}{\partial E}|_E$ and $\mathcal{A}''(E) = \frac{\partial^2 \mathcal{A}}{\partial E^2}|_E$. One then obtains

$$\bar{\mu} = (\mathcal{A}(E) - \alpha_0) \Delta B^2(E) + \delta E^2 \left[(\mathcal{A}(E) - \alpha_0) (B'(E))^2 + \frac{1}{2} \mathcal{A}''(E) \Delta B^2(E) \right], \quad (16)$$

where we isolated the corrections proportional to δE^2 . If \hat{B} is a local operator, these corrections are suppressed by a factor of N compared to the first leading term. On the other hand, when \hat{B} is a sum of local operators, then the correction (proportional to $B'(E)$) scales with N in the same way as the first leading term.

3.3 Existence of a parametric window for the echo growth

We are now in the position to compare the short and the long-time behavior and find the conditions under which there is a parametric window for the echo's growth. A simple qualitative criterion for the existence of such a window is

$$|\mu(t^*)| \sim N^{-\ell} |\bar{\mu}|,$$

where ℓ is a positive power and t^* is the time of breakdown of the short time expansion. We will focus only on a class of operators \hat{A} and \hat{B} , which are either local in spins or can be represented as sums of local terms, i.e. we will focus on most common and measurable operators representing physical observables. In addition, we will also assume that the Hamiltonian contains sums of few spins (fermion) terms, i.e. it can contain an external field and two or three spin interactions, which may not necessarily be local in space. Under these assumptions, the Hamiltonian can flip at most few spins. Therefore, for the states connected by the nonzero matrix element $|H_{0\lambda}|^2$, the differences $\alpha_\lambda - \alpha_0$ and $\beta_\lambda - \beta_0$ are non-extensive irrespective whether \hat{A} or \hat{B} are local or are sums of local terms. Therefore $|\alpha_\lambda - \alpha_0|$ and $|\beta_\lambda - \beta_0|$ are bounded by some non-extensive constants $M_A = \text{Max}_\lambda |\alpha_\lambda - \alpha_0|$ and $M_B = \text{Max}_\lambda |\beta_\lambda - \beta_0|$. In order to estimate the short time expansion using Eq.(6), let us now distinguish three different possibilities, which we discuss one by one: (i) both \hat{A} and \hat{B} are collective operators, (ii) one of the operators is global one is local and (iii) both \hat{A} and \hat{B} are local.

(i) \hat{A} and \hat{B} are global operators. In this case at short times

$$\begin{aligned} \mu(t) &\leq t^2 \sum_{\lambda \neq 0} |\hat{H}_{0\lambda}|^2 |\beta_\lambda - \beta_0|^2 |\alpha_\lambda - \alpha_0| \\ &\leq t^2 M_A M_B^2 \sum_{\lambda \neq 0} |\hat{H}_{0\lambda}|^2 \sim Ct^2 N, \end{aligned} \quad (17)$$

where we used the standard normalization of the Hamiltonian such that it has an extensive energy variance

$$\langle \psi_0 | \hat{H}^2 | \psi_0 \rangle = \sum_{\lambda} |\hat{H}_{0\lambda}|^2 \propto N.$$

We note that this scaling with N can be reduced further if $\alpha_\lambda - \alpha_0$ has an alternating sign between different eigenstates α_λ . The time t^* defining the validity of the short time expansion can be estimated from the decay of the expectation value of $\hat{B}(t)$, which is readily obtained from Eq. (5)

$$\langle \psi_0 | \hat{B}(t) | \psi_0 \rangle = \beta_0 + t^2 \sum_{\lambda} |H_{0\lambda}|^2 (\beta_\lambda - \beta_0) + O(t^3).$$

By equating the first and the second term in the expansion and by the same arguments of extensivity of the energy variance in the initial state we see that the time t^* is N -independent.

(ii) Either \hat{A} or \hat{B} is local, the other is extensive. In this case locality of one of the operators \hat{A} or \hat{B} (let us say \hat{B} for concreteness) restricts the eigenstates $|\alpha_\lambda\rangle$ in Eq. (17) to those where one of the local degrees of freedom (e.g. a spin) is localized. This additional selection rule removes a factor of N from the the sum in Eq. (17) leading to the following estimate

$$\mu(t) \sim Ct^2, \quad (18)$$

It is easy to see that the time scale t^* does not depend on whether the operator \hat{B} is extensive or not remaining N -independent also in this case.

(iii) *Both \hat{A} and \hat{B} are local.* We will focus on operators that are not spatially separated. The OTOC for spatially separated operators was analyzed in the literature, see e.g. Ref. [48]. In these situations, there is a possibility for exponential echo growth, related to the out of the light cone dynamics and not generally connected to the existence of chaos. Assuming that there is no spatial separation, we can easily check that the Eq. (18) still holds.

Let us now determine the long time asymptotes of $\mu(t)$ from Eq. (9) for the three cases. As already mentioned, this sets a condition for the initial state and operator \hat{A} , namely we require that the initial state in Eq.(3) is such that the difference between the initial value and its long time limit $\mathcal{A}(E) - \alpha_0$ appearing in Eq.(16) is maximal. In the case of global operator \hat{A} , we ask for an extensive difference, then we immediately find for Eq. (9) that for the case (i) $\bar{\mu} \propto N^2$. Likewise for the case (ii), i.e. when either \hat{A} or \hat{B} is an extensive operator we have $\bar{\mu} \propto N^1$ and finally for the case (iii) $\bar{\mu} \propto N^0$. Comparing these asymptotes with the short time expansions of $\mu(t)$ discussed above we see that in order to have a non-perturbative growth of echo one should chose either the possibility (i) or (ii), i.e. at least one of the two operators \hat{A} or \hat{B} should be extensive. In particular a very convenient choice we will use most is (i) where $\hat{A} = \hat{B}$ are the global magnetization along a particular direction:

$$\hat{A} = \hat{S}^\alpha = \sum_{i=1}^N \hat{\sigma}_i^\alpha \quad \text{with} \quad \alpha = x, y, z . \quad (19)$$

This choice is analogous to the one used in Refs. [21] and [33] and with that of standard echo-experiments [17–20]. We will also show results for other cases ((ii) and (iii)).

4 The Sherrington-Kirkpatrick model in transverse field

We will now corroborate our general discussion with an analysis of the Sherrington-Kirkpatrick (SK) model, describing a set of spins with infinite-range interactions in their z -components. To make this model dynamical we add a uniform transverse field. Below we will also analyze a version of this model with local interactions which decay in space according to a Gaussian law.

The Hamiltonian of the SK model in the transverse field reads

$$\hat{H} = -\frac{1}{2} \sum_{i \neq j}^N J_{ij} \hat{\sigma}_i^z \hat{\sigma}_j^z - h \sum_{i=1}^N \hat{\sigma}_i^x , \quad (20)$$

where $\hat{\sigma}_i^z, \hat{\sigma}_i^x$ are the Pauli matrices and the couplings J_{ij} are random symmetric numbers distributed according to the Gaussian probability with zero mean and the variance J^2/N as

$$J_{ij} = \frac{J}{\sqrt{N}} g_{ij} , \quad (21)$$

where g_{ij} are Gaussian random numbers with zero average and unit variance. At equilibrium, the phase-diagram of the SK model has been extensively studied [34–36]. In the limit of

zero transverse field ($h = 0$), one recovers the classical SK model, [49, 50] which has a glass transition at the critical temperature $T_c = J$. The SK model in transverse field has a zero-temperature quantum phase transition at a critical magnetic field $h_c(T = 0) \sim 1.52J$. [35] Away from equilibrium, this model was explored in Refs. [51–54]. Recently, the SK model has been also considered in the context of scrambling in Ref. [37], as a natural setup to access the square commutator via interferometry in cold-atoms experiments. See also Refs. [55, 56] for related models.

In what follows, we will also analyze a *short-range version* of the SK model. It is described by the same spin Hamiltonian (20), but the random couplings J_{ij} connecting the sites i, j now decay with the distance r_{ij} according

$$J_{ij} = \frac{J}{\sqrt{N(\sigma)}} e^{-\frac{r_{ij}^2}{2\sigma^2}} g_{ij}, \quad (22)$$

where σ is a parameter defining the interaction range. In one dimension with periodic boundary conditions the distance between any two sites is taken to be $r_{ij} = \min(|i - j|, N - |i - j|)$. We normalized the couplings by the effective number of spins within the correlation length σ : $N(\sigma) = \sum_{i \neq j} e^{-r_{ij}^2/2\sigma^2} / N \sim \sqrt{\pi}/2 \sigma \text{Erf}(N/\sigma)$. This choice correctly interpolates between the short range ($\sigma \approx 1$) and the long range ($\sigma \rightarrow \infty$) limits of the SK model always keeping the energy variance extensive. In the infinite range limit $\sigma \rightarrow \infty$, the standard SK model is recovered (21) and $N(\sigma) = N$. In the opposite case when $\sigma \ll N$, the normalization is simply a constant $N(\sigma) \sim 2/\sqrt{\pi} \sigma$.

5 Truncated Wigner Approximation (TWA) in the large N -limit

In order to study quantum dynamics approaching the thermodynamic limit, we will combine exact diagonalization with the semi-classical *truncated Wigner approximation* (TWA) [38–41, 57, 58]. For completeness, we briefly outline the application of the latter method to the SK model.

Within the TWA (like in any other phase space formalism) one first identifies a complete set of quantum operators forming a closed algebra, i.e. closed commutation relations, with a corresponding set of canonical phase-space variables [41, 57–60]. Then, any quantum operator including the initial density matrix can be mapped to a function of phase-space variables via the Wigner-Weyl transform. The dynamics are then described by deterministic nonlinear classical Hamiltonian equations of motion, which correspond to the saddle point of the action in the Feynman’s path integral representation of the time evolution [41]. Formally these equations are obtained from the quantum Heisenberg equations by replacing the operators with the corresponding Weyl transforms and the commutators with the Poisson brackets multiplied by the imaginary unit. Within the TWA quantum fluctuations are encoded in the initial Wigner function (the Weyl transform of the density matrix).

In quantum systems with a well defined classical limit, like a particle in an external potential or a system of spins with large angular momentum, the TWA is known to asymptotically describe quantum echoes at short times. This approach breaks down eventually at the so-called *Ehrenfest time* t_{Ehr} , when quantum interference effects between classical trajectories become significant [14, 27, 61, 62]. Interestingly, TWA for the forward evolution of observables

usually works for much longer times. This suggests that the quantum echo is a very sensitive probe defining the crossover time scale separating classical and quantum time evolution. This time-scale t_{Ehr} typically diverges as we approach the classical limit. In particular, for a particle in a chaotic potential, it is known to be

$$t_{\text{Ehr}} = \frac{1}{2\lambda_{\text{max}}} \log \frac{1}{\hbar}, \quad (23)$$

where $\lambda_{\text{max}} > 0$ is the maximal Lyapunov exponent of the classical dynamics [63]. For non-linear spins the role of $1/\hbar$ is played by the spin size S and the Ehrenfest time diverges as $\log(S)$. In the case of many-body fully interacting models (like the SK), the validity of the semiclassical approximation is less understood. In equilibrium, the large N -limit ensures the validity of the saddle point mean-field approximation, so it is natural to expect that $1/N$ serves as an effective \hbar , as it was indeed shown to be the case for the SYK model [26].

5.1 TWA for the SK model

We obtain a phase space representation by mapping the spin operators on each site $\hat{s}_i^\alpha = \hat{\sigma}_i^\alpha/2$ with $\alpha = x, y, z$ and $i = 1, \dots, N$ to the classical spin variables s_i^α . These spin variables form the $3N$ -dimensional phase space. They satisfy the standard angular momentum Poisson bracket relations: $\{s_i^\alpha, s_j^\beta\} = \delta_{ij} \epsilon_{\alpha\beta\gamma} s_i^\gamma$, where $\epsilon_{\alpha\beta\gamma}$ is the Levi-Civita symbol. Clearly these Poisson brackets correspond to spin commutation relations of the corresponding spin operators.

The Weyl symbol of the Hamiltonian (20) is simply

$$\mathcal{H} = -2 \sum_{i \neq j}^N J_{ij} s_i^z s_j^z - 2h \sum_{i=1}^N s_i^x, \quad (24)$$

with J_{ij} the same random couplings as in Eq.(21). The equations of motion for the spin variables $\vec{s}_i = (s_i^x, s_i^y, s_i^z)$ are obtained from the Poisson brackets¹ with Eq.(24) as

$$\frac{d\vec{s}_i}{dt} = \{\mathcal{H}, \vec{s}_i\} = -\vec{s}_i \times \frac{\partial \mathcal{H}}{\partial \vec{s}_i} \quad (25)$$

and correspond to the mean-field Heisenberg equations of motion of the quantum Hamiltonian (20).

For simplicity we will consider simple product initial states $|\psi_0\rangle$, whose Wigner function $W(\{s_i^\alpha(0)\})$ also factorizes. Instead of the exact Wigner function we will choose its Gaussian approximation, where its first and the second moments are fixed by the mean and the variance of the corresponding quantum spin operators in the initial state:

$$\langle \psi_0 | \hat{s}_i^\alpha | \psi_0 \rangle = \overline{s_i^\alpha(0)}, \quad \langle \psi_0 | \hat{s}_i^\alpha \hat{s}_i^\beta | \psi_0 \rangle = \overline{s_i^\alpha(0) s_i^\beta(0)}, \quad (26)$$

¹Spin Poisson brackets are defined as $\{f, g\} = \sum_i \epsilon_{\alpha\beta\gamma} \frac{\partial f}{\partial s_i^\alpha} \frac{\partial g}{\partial s_i^\beta} s_i^\gamma$, where $\epsilon_{\alpha\beta\gamma}$ is the antisymmetric Levi-Civita tensor and the sum is repeated over the indices $\alpha, \beta, \gamma = x, y, z$.

for $\alpha = x, y, z$. The double over-line here represents averaging with respect to the Wigner function. As an example, the initial state $|\psi_0\rangle = |\downarrow\downarrow\dots\downarrow\rangle$ corresponds to

$$\overline{\overline{s_i^z(0)}} = -1/2, \quad \overline{\overline{s_i^{x,y}(0)}} = 0, \quad \overline{\overline{s_i^\alpha(0)s_i^\beta(0)}} = \frac{1}{4}\delta_{\alpha\beta}.$$

This matching can be achieved for any product initial state [60] such that within this approximation the Wigner function remains positive. The Gaussian Wigner function has the advantage that it is positive definite and easy to sample. Also, generally, the accuracy of the TWA is set by the second power of the effective Planck's constant, which is the same as the accuracy of the Gaussian approximation of the Wigner function [60]. Alternatively one can use a discrete Wigner function [57,58], which is also positive and which accurately describes all the moments of the spin operators in the initial state. We checked numerically that the results obtained using the Gaussian and the discrete Wigner functions do not have any noticeable differences. We integrate numerically Eq.(25) and average at each time t over N_{samp} trajectories, whose initial conditions are distributed according to the initial Wigner function (26). For numerical integration, we use an adaptive fourth-order Runge-Kutta algorithm, fixing the error to 10^{-12} .

Before analyzing the echo, let us consider the magnetization dynamics (19) with forward

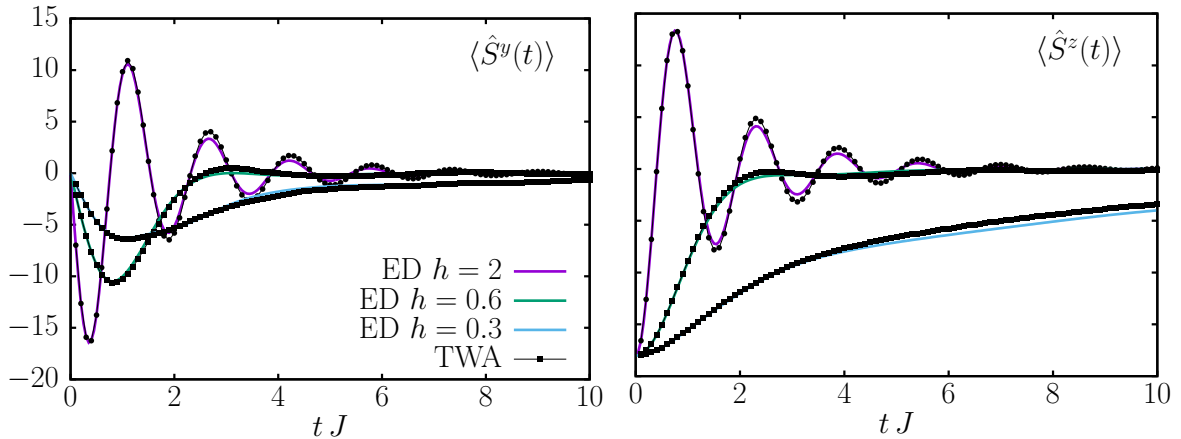


Figure 1: Comparison of TWA results to exact magnetization dynamics with SK couplings (21) for a fixed disorder realization at different transverse fields h for $N = 18$ spins. The top panel shows the magnetization along y $\langle \hat{S}^y(t) \rangle$, while the bottom one the magnetization along z $\langle \hat{S}^z(t) \rangle$. Full lines ED simulations, dotted lines correspond to TWA simulations with $N_{samp} = 8000$.

evolution, where we suddenly quench the system to the SK Hamiltonian (24). We check the validity of TWA by comparing it with exact diagonalization (ED)². In what follows, we focus for concreteness on the initial product state where all spins are polarized along the z -axis: $|\psi_0\rangle = |\downarrow\downarrow\dots\downarrow\rangle$, but the validity of the method does not depend on this choice. In Fig. 1, we show results of the time evolution of the total spin components along the y and z axes for a fixed realization of the spin-spin couplings in the SK Hamiltonian. As expected, TWA gives

² We address the exact quantum dynamics by employing the the method of Krylov sub-spaces in order to avoid full diagonalization, see i.e. Ref. [64].

an excellent quantitative description of the forward time evolution of the magnetization for all simulated times and for different values of the transverse field h , irrespectively of the phase of the Hamiltonian. This shows that the validity of TWA does not depend on the glassiness of the model. Furthermore, by increasing the system size N , TWA asymptotically reproduces the exact quantum dynamics. This is shown in Fig.2, where we compare TWA to ED for fixed h increasing N . In the inset of the same figure, we plot the absolute value of the difference between the two results $\text{Diff}(\langle S_z(t) \rangle)$, which goes to zero in the thermodynamic limit.

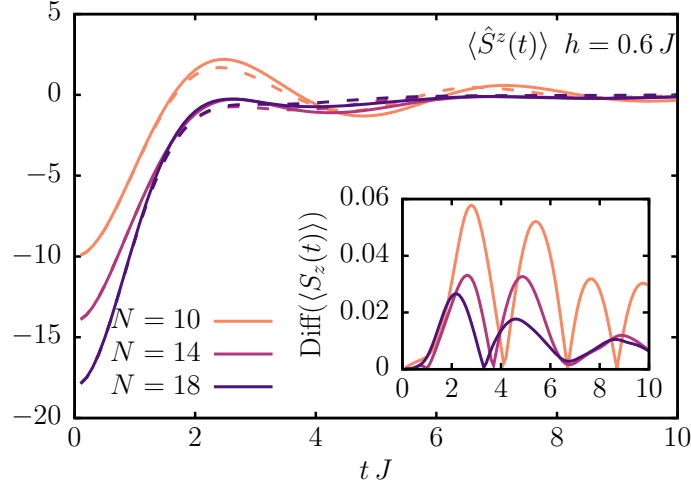


Figure 2: Comparison between ED (solid lines) and TWA (dashed lines) dynamics for $\langle \hat{S}^z(t) \rangle$ with SK model (21) for a fixed disorder realization and fixed $h = 0.6 J$ with different $N = 10, 14, 18$. In the inset we plot the absolute value of the difference between the two results. TWA simulations with $N_{\text{samp}} = 8000$.

As evident from the data, the TWA error reaches the maximum at an intermediate, system size-independent time before decreasing again at late times. The maximal error diminishes with N . It is interesting that there is no clear signature of the Ehrenfest t_{Ehr} time in the forward evolution such that at sufficiently large N the TWA correctly reproduces the magnetization dynamics at all times. This is to be contrasted with the echo dynamics, analyzed in the next section, where we will see that TWA breaks down after t_{Ehr} , which for these parameters and largest analyzed $N = 20$ is given by $Jt_{\text{Ehr}} \approx 2$ (c.f. Fig. 5).

5.2 TWA for the short-range model

In the case of the short-range Hamiltonian, the TWA approach is the same as the one illustrated in the previous section, with the only difference of the short-range couplings as given by Eq.(22). In this case, $1/N(\sigma) \sim 1/\sigma$ acts as an effective \hbar and TWA is expected to fail at a time-scale set by σ , which is N -independent. In the short-range limit, for fixed finite σ , the semi-classical approximation does not reproduce the exact quantum dynamics in the thermodynamic limit. Indeed, in Fig.3(a.), we show the comparison of the TWA with the ED dynamics for $\langle \hat{S}_z(t) \rangle$ from the initial state $|\psi_0\rangle = |\downarrow\downarrow\dots\downarrow\rangle$ at fixed $\sigma = 1$ varying $N = 10 \div 18$. The results might seem qualitatively in agreement with the exact dynamics. However, they do not improve increasing the system size, as shown in the inset. On the other hand, when $N(\sigma) \sim \sigma$ is big enough, TWA is accurate also at long-times. In fact in Fig.3(b.),

we plot $\langle \hat{S}_z(t) \rangle$ at fixed $N = 18$ for different $\sigma = 1, 2, 6$. The difference between ED and TWA (displayed in the inset) shows how the reliability of TWA grows by increasing σ at fixed N .

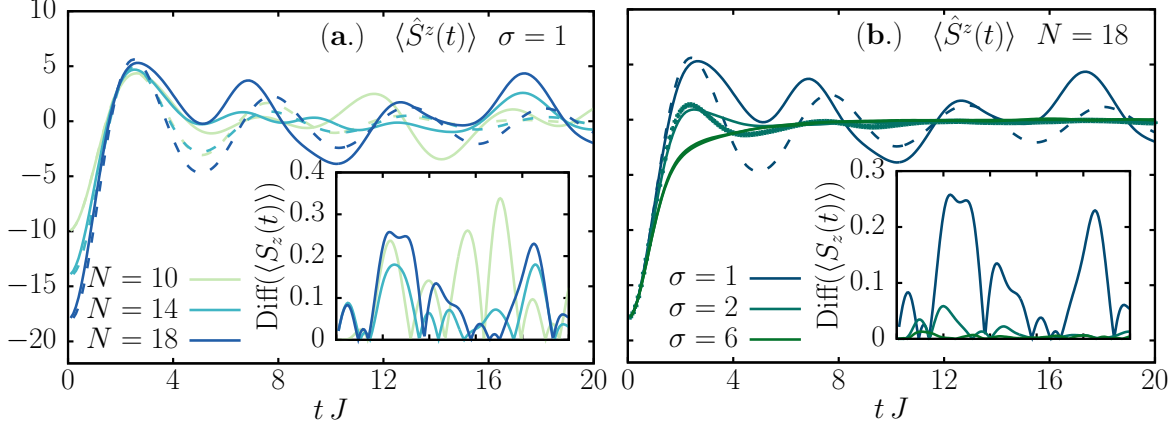


Figure 3: Comparison of ED (solid lines) and TWA (dashed lines) dynamics of $\langle \hat{S}^z(t) \rangle$ for a single realization of the short-range Gaussian couplings (22) at $h = 0.6J$. TWA breakdown is set by $N(\sigma) \sim \sigma$, which is N -independent. (a.) Short-range couplings for fixed $\sigma = 1$ with different $N = 10, 14, 18$. In the inset, we plot the absolute value of the difference between the two results as a function of time. (b.) Same as in (a) but for fixed $N = 18$ and different range of interactions $\sigma = 1, 2, 6$. TWA simulations with $N_{\text{samp}} = 8000$.

6 Scrambling in the SK model

Let us now turn to the dynamics of the echo and hence OTOC in the SK model and in its short-range version. In particular, we will study numerically the role of the number of spins N , the choice of the operator and of the range interactions for both observing the exponential growth of OTOC and for the validity of the semiclassical TWA approach. We first discuss the echo dynamics under the evolution of the all-to-all SK Hamiltonian with Eq.(20).

Let us start by discussing the choice of the operators \hat{A} and \hat{B} according to the cases (i), (ii) and (iii) discussed in Sec. 3. We focus for definiteness on magnetization along the z axis. We consider (i) extensive-extensive $\hat{A} = \hat{B} = \hat{S}^z = \sum_j \hat{\sigma}_j^z$ [c.f. Eq. (19)], (ii) extensive-local $\hat{A} = \hat{S}^z$ with $\hat{B} = \sigma_i^z$ and (iii) local-local $\hat{A} = \hat{B} = \hat{\sigma}_i^z$, where the site i is chosen randomly for each disorder realization. Notice that another possibility for (ii) discussed in Sec. 3 is $\hat{A} = \hat{\sigma}_j^z$ local with $\hat{B} = \hat{S}^z$ extensive. This possibility in fact yields results identical to those of (i) with the $\langle A(t) \rangle$ and $\mu(t)$ simply scaled down by a factor of N . This follows from the fact that the expression for the echo (2) is linear in \hat{A} . We will also choose a fully polarized product initial state $|\psi_0\rangle = |\downarrow\downarrow \dots \downarrow\rangle$, which automatically satisfies the requirement (16) and maximizes the difference between the initial and asymptotic value $\mathcal{A}(E) - \alpha_0 \sim -\alpha_0$ [c.f. Eq.(16)]. In fact, the energy of this fully polarized state, which is generic and suitable for studying the echo dynamics, lies in the middle of the spectrum of the Hamiltonian, therefore $\mathcal{A}(E) \sim 0$. At early times the echo grows quadratically as predicted by Eq.(6), which in

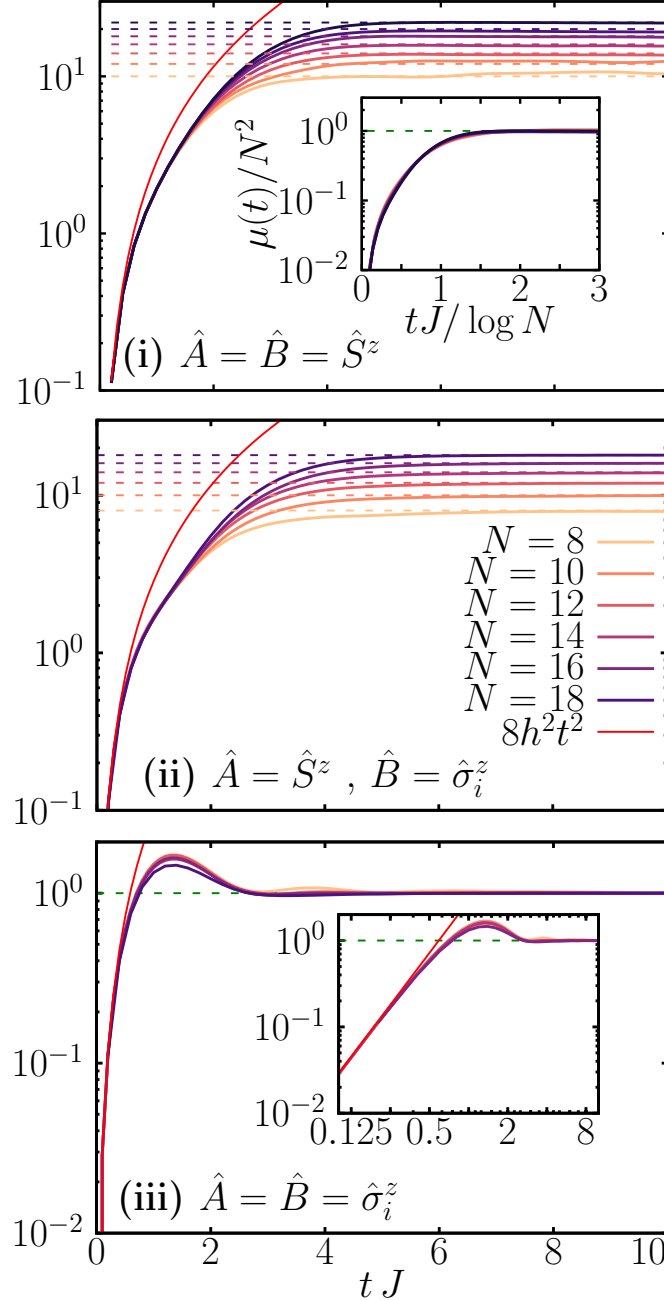


Figure 4: Exact scrambling dynamics $\mu(t)$ for different observables realizing (i.-iii.) of Sec.3.3, for system size $N = 8 \div 18$ increasing color intensity. The early time quadratic growth is plotted in red, while the saturation value as predicted by ETH [cf. Eq.(9)] illustrated by the dashed lines. (Left panel) (i) $\mu(t)/N$ for extensive-extensive operators $\hat{A} = \hat{B} = \hat{S}^z$. (Center panel) (ii) $\mu(t)$ for extensive-local operators $\hat{A} = \hat{S}^z$ with $\hat{B} = \hat{\sigma}_i^z$. (Right panel) (iii) $\mu(t)$ for local-local $\hat{A} = \hat{B} = \hat{\sigma}_i^z$. (i-ii) Changing N , the echo keeps growing — exponentially fast in the limit $N \gg 1$ — eventually saturating to a value $\mu \sim N^2$ (dashed lines). In the inset of (i) we show $\mu(t)/N^2$ as a function of the rescaled time $tJ/\log N \sim tJ/t_{\text{Ehr}}$ showing the long time scaling collapse of the echo for different values of N . (iii) The echo saturates to unity (green dashed line), while in the inset the same data are plotted in a doubly logarithmic scale. The results correspond to a fully polarized initial state with $h = 0.6 J$, averaged over 50 disorder realizations (see text for details).

this case can be computed explicitly yielding (i) $\mu(t) = 8 N h^2 t^2$ and (ii-iii) $\mu(t) = 8 h^2 t^2$. This perturbation expansion breaks down at $t^* \sim 1/\sqrt{J^2 + 4h^2}$. After t^* , $\mu(t)$ enters a non-perturbative regime, until it saturates at long-times to the value: (i) $\bar{\mu} \approx N^2$, (ii) $\bar{\mu} \approx N$, (iii) $\bar{\mu} \approx 1$, as immediately follows from Eq. (9) for an infinite temperature state which has no magnetization correlations between different spins. This general behaviour is exemplified in Fig.4, where we show the exact quantum dynamics of the echo observable for (i-iii) for finite system sizes up $N = 8 \div 18$ for $h = 0.6 J$, averaged over 50 disorder realizations. The figure shows how the early time quadratic growth — red in the plot — breaks at a time, which is N -independent. For (i-ii), the saturation value predicted by ETH is represented by dashed lines for each N at the corresponding colour, displaying the existence of a parametric window that scales with N that gives “room” for chaos to develop. On the other hand, the panel (iii) shows the saturation of the echo to one (green dashed line) leading the same dynamical behaviour of the echo independently of N .

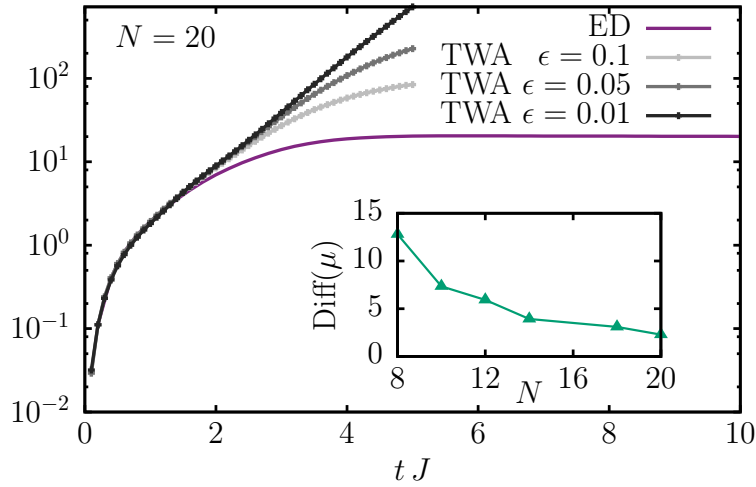


Figure 5: Comparison between the TWA scrambling dynamics $\mu(t)/N$ and the exact results at $N = 20$ varying ϵ . An exponential fit of the TWA data for $\epsilon = 0.01$ with $f(x) = ae^{2\Lambda x}$ yields the exponent $2\Lambda = 1.5/J$. In the inset we show the difference between the TWA and ED results at fixed time $t = 2$ as a function of the system size N . By increasing N , the exact results approach the TWA exponential growth before saturation. The results correspond to a fully polarized initial state with $h = 0.6 J$ for a single disorder realizations. TWA with $N_{\text{samp}} = 20000$.

Let us now focus on the case (i) for $\hat{A} = \hat{B} = \hat{S}^z$. By increasing N , the non-perturbative time-regime extends and the late time dynamics collapses if we plot $\mu(t)$ vs $tJ/\log(N)$, as shown in the inset of the same Fig.4 (i). This time-scale is compatible with the Ehrenfest time defined in Eq.(23), meaning that the echo has an asymptotic form $\mu(t) = N^2 f(tJ/t_{\text{Ehr}})$. Hence the intermediate, non-perturbative regime extends for $t^* < t < t_{\text{Ehr}}$, the latter being divergent in the thermodynamic limit, and it is compatible with exponential growth.

In order to study the $\mu(t)$ dynamics before the Ehrenfest time, we resort to TWA. As discussed in Sec.5.1, for this model the semi-classical approach correctly describes the expectation value of the observables in this time-regime. In Fig.5, we show TWA results in comparison with ED, for a single-disorder realization at finite size $N = 20$. After a short

transient time, the TWA data exhibit a clear exponential growth, whose extent is determined by the parameter ϵ , representing the strength of the perturbation, see Eq.(1). This situation is analogous to what happens in chaotic classical systems with compact phase-space. There, the ratio between the distance of two nearby trajectories, initially separated by ϵ , ultimately saturates at a typical value fixed by the available phase space separation. For larger ϵ this saturation happens earlier, hence there is a shorter domain of exponential growth. The difference between exact ED and TWA data at fixed time, $\text{Diff}(\mu)$ goes down with the system size as indicated in the inset of Fig.5. This result is consistent with the asymptotic accuracy of the TWA in the large N -limit, as discussed above for the magnetization. However, for long times, unlike for the magnetization, this difference can be arbitrarily large as $\epsilon \rightarrow 0$.

TWA has an interesting advantage over the ED in the fact that it allows to accurately extract the exponent characterizing the growth of the echo even for relatively small system sizes (see also Ref. [26] for the related discussion on the SYK model). In the case of the transverse field $h = 0.6 J$ as in Fig. 5, an exponential fit yields $2\Lambda \sim 1.5/J$, while in general Λ is an increasing function of h . The rate Λ (sometimes referred to as the generalized Lyapunov exponent [65–67]) is related to the maximal Lyapunov exponent of the theory λ_{max} [21, 26]. The difference between the two comes from the different order of operations of taking logarithm and ensemble averaging. Exactly the same considerations apply in the case of other observables, i.e. magnetization in the other directions \hat{S}^x, \hat{S}^y , see the Appendix A for further examples.

6.1 Absence of exponential sensitivity with short-range interactions

The exponential sensitivity of the echo disappears in the presence of local interactions. This happens simultaneously with the failure of the semi-classical TWA approximation. Thus for the SK Hamiltonian with short-range Gaussian couplings (22) for the same polarized initial state, short-range interactions result in at most a power-law growth of echo, in accordance with what was first observed in Ref. [21] and then proved in Ref [33]. In Fig. 6, we show the quantum ED evolution for a fixed system size at different values $\sigma = 1, 2, 6$ and compare them to the corresponding TWA results. As the plots show, for the short-range model $\sigma = 1, 2$ the echo growth according to the initial perturbative power until it crossovers to a slower polynomial growth best fitted by $\mu(t) \propto t^{0.5}$ consistent with Refs. [21, 33] (see the inset) and the eventual saturation to the correct ETH value Eq. (15). As σ increases one can observe a slow emergence of the non-perturbative intermediate time dynamics of fast echo growth, which is expected to crossover to the exponential growth in the limit $\sigma \rightarrow \infty$. From this plot it is also evident that the TWA fails after a shorter (N -independent) time, incorrectly showing the persistence of exponential growth of the echo even for the short-range model. These results can be re-phrased by saying that the effective Ehrenfest time becomes of the same order as the time of breakdown of the short time expansion, i.e. $t_{\text{Ehr}} \sim t^*$, leading to a lack of the semi-classical time-window necessary for the exponential quantum growth of the echo. Remarkably, the presence of short-range interactions leads to the absence of exponential regime, which is replaced by a much slower non-perturbative growth than the corresponding semi-classical limit.

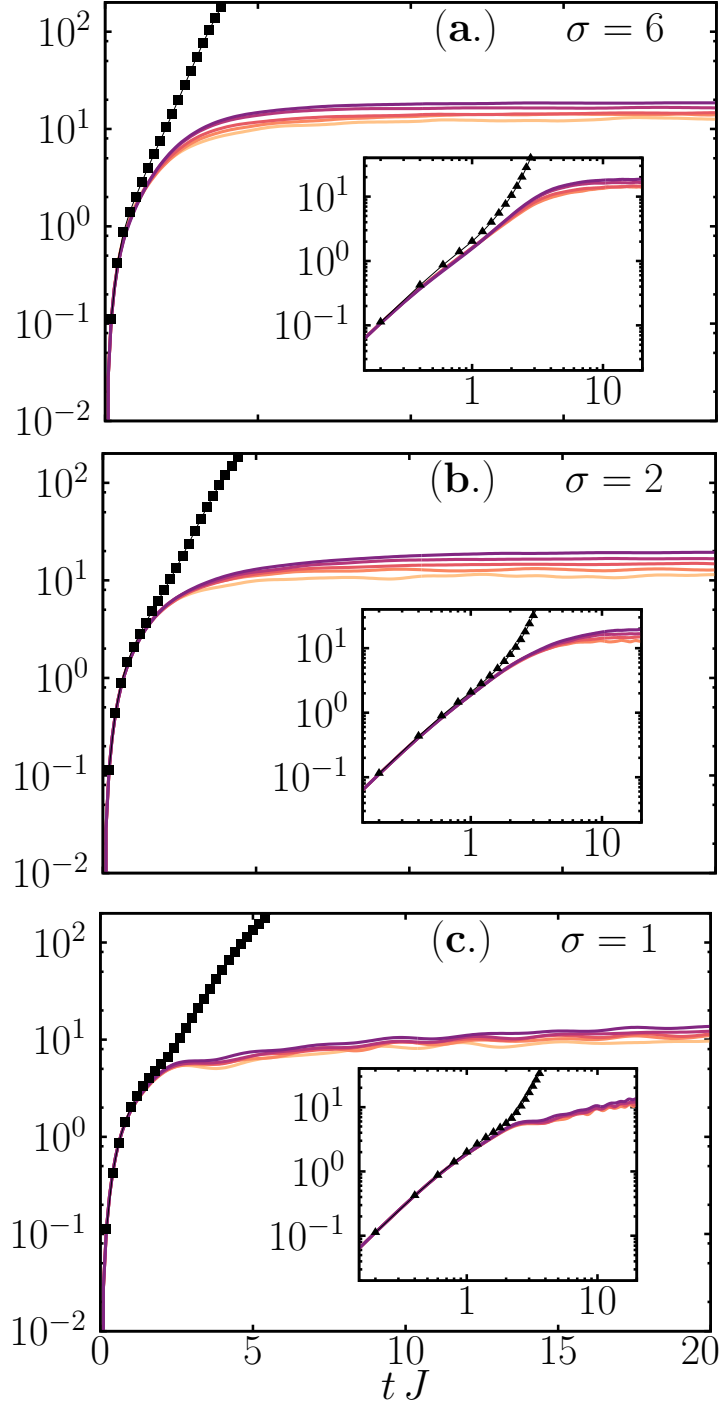


Figure 6: Absence of the exponential growth for the scrambling dynamics induced by short range couplings (22) for different σ . We compare exact quantum ED dynamics for different system sizes $N = 8 \div 16$ (increasing color intensity) with TWA results for $N = 16$ and $\delta = 10^{-2}$ (dotted black lines). The range of interaction is decreased choosing $\sigma = 6, 2, 1$ in the panels (a.), (b.) and (c.) respectively. The results correspond to a fully polarized initial state with $h = 0.6 J$, averaged over 50 disorder realizations (see text for details).

7 Discussion

In this work, we have studied the quantum echo dynamics and its exponential divergence in time in the Sherrington-Kirkpatrick model with transverse field. We have shown that, by choosing collective observables and an initial state such that the initial value of the observable is extensively bigger than its stationary value, the echo grows exponentially, with the same rate of the underlying semi-classical theory. On the other hand, the presence of short-range interactions results in the absence of exponential sensitivity in the quantum dynamics [21, 43] as a result of the lack of a well defined semi-classical limit. In this case, understanding the nature of the non-perturbative polynomial regime remains an open question, beyond the scopes of the present work.

Overall, we would like to emphasize that the echo (and the OTOC in general) can be used as a precise probe of failure of a classical analysis, exactly in the spirit of the seminal paper by Larkin and Ovchinnikov [14]. Indeed, the forward evolution of observables, i.e. magnetization, is reproduced by semi-classical approximations up to times which go beyond t_{Ehr} and can even extend all the way to infinity. Conversely, the semiclassical description of the OTOC breaks down precisely at t_{Ehr} and it allows one to clearly identify the Ehrenfest time as the breakdown time of the classical evolution.

Because of the connection between the echo (or the square commutator) to the expectation value (or the variance) of the observables under effective time reversal, our findings are directly relevant to experiments allowing one to access exponential signatures of chaos in atomic experiments. A more general and open question concerns the full distribution of the echo operator. We observed numerically that higher cumulants of the echo signal produce deviations between the ED and the TWA predictions even before the Ehrenfest time. We will leave this analysis for future work.

Acknowledgements

We acknowledge useful discussions with Rosario Fazio, Efim Rozema, Antonello Scardicchio, Markus Schmidt, Dries Sels, Xhek Turkeshi and Jonathan Wurtz. We thank the facilities of the Boston University Shared Computing Cluster, over which we run all the numerical simulations.

Funding information Research of A.P. was supported by A.P was supported by NSF DMR-1813499 and AFOSR FA9550-16-1-0334. SP thanks Boston University's Condensed Matter Theory Visitors program for support. Part of this work has been carried out during the workshop "Breakdown Of Ergodicity In Isolated Quantum Systems" at the Galileo Galilei Institute (GGI) in Florence.

A Echo dynamics for the magnetization along y

In Sec.3, we argued that the choice of the initial state to respect to the observable is crucial in order to ensure space for chaos to develop and in Sec.6 we showed the results of its exponential growth for \hat{S}_z . Below, we show the same analysis for the equivalent operators \hat{S}^x , \hat{S}^y .

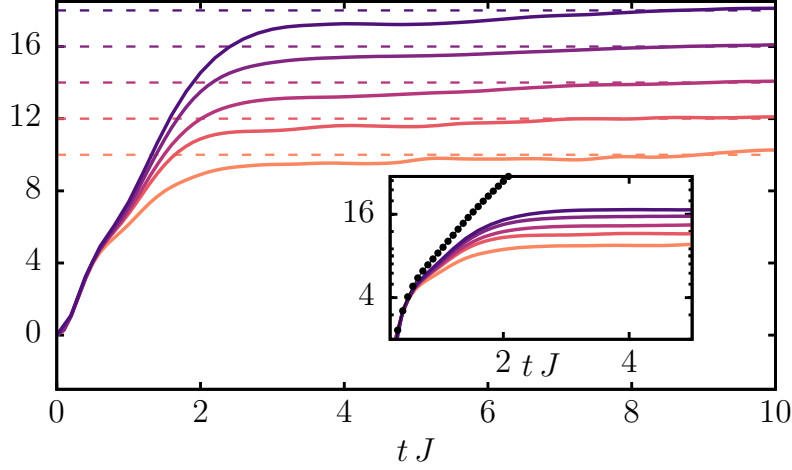


Figure 7: Exact scrambling dynamics $\mu(t)/N$ with the SK hamiltonian (20) for $\hat{A} = \hat{B} = S^y$ for $N = 10 \div 18$ increasing color's intensity. Dashed in the plot the ETH saturation value for finite N . In the inset the data are plotted in a semi-log scale to display the exponential growth before saturation. An exponential fit of the TWA data with $f(x) = ae^{2\Lambda x}$ yields the exponent $2\Lambda \simeq 1.1/J$. The results correspond to a fully polarized initial state in the y direction with $h = 0.1 J$, for 50 disorder realizations.

Let us first consider $\hat{A} = \hat{B} = \hat{S}^y$ with the initial state $|\phi_0\rangle = |LL\dots L\rangle$ fully polarized in the y direction ($\hat{\sigma}_i^y |L\rangle_i = -|L\rangle_i$). As for the z direction, also the energy E of $|\phi_0\rangle$ lies the middle of the spectrum, hence the magnetization along the y always vanishes at long-times, i.e. in Eq.(16) the difference $\mathcal{S}^y(E) - S_0^y \simeq -S_0^y$ is maximized. Therefore the same conclusions of Sec.6 for \hat{S}^z hold in this case. The resulting behaviour is exemplified in Fig.7, where we show the exact quantum dynamics of the echo observable at finite system size up $N = 8 \div 16$ for $h = 0.1$, averaged over 50 disorder realizations.

On the other hand, for $\hat{A} = \hat{B} = \hat{S}^x$ with $|\chi_0\rangle = |+\dots+\rangle$ ($\hat{\sigma}_i^x |+\rangle_i = |+\rangle_i$) the situation slightly changes. In this case, the Hamiltonian (20) has a transverse field in the x -direction, and $\langle \hat{S}^x(t) \rangle$ attains a non-vanishing value at long-times, which changes the stationary value of the echo (9). With this choice of the initial state, we have $\alpha_0 = S_0^x = N$. Anyhow, by choosing a small transverse field, the dynamics is such that $\mathcal{S}^x(E)$ is still finite (but small) and the difference $\mathcal{S}^x(E) - \alpha_0$ not only is extensive, but big enough to appreciate the exponential growth with exact numerics for small system sizes. The echo dynamics is displayed in Fig.8, where we show the exact quantum dynamics of the echo observable at finite system size up $N = 8 \div 18$ for $h = 0.2$, averaged over 50 disorder realizations. By increasing N , the ED results approach the TWA semi-classical dynamics, characterized by the exponent $2\Lambda \simeq 1.3$. In the insets we show how the saturation value $\overline{S^x} \simeq \mathcal{S}^x(E)$ affects the echo's saturation, leading to $\overline{\mu} \sim N (\mathcal{S}^x(E) - \alpha_0)$.

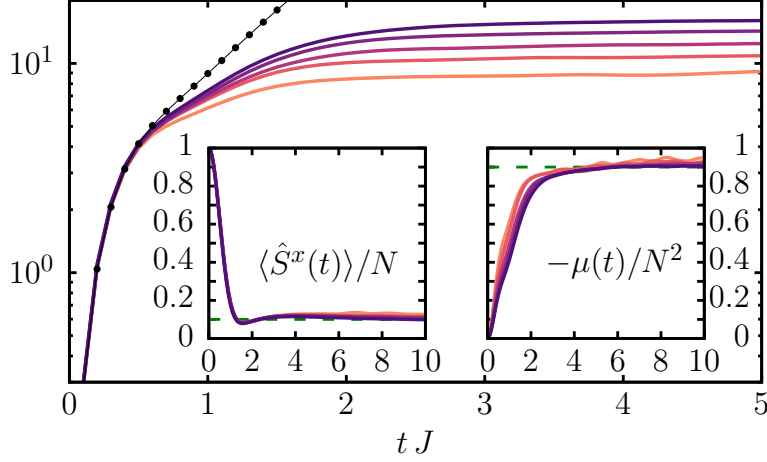


Figure 8: Echo dynamics $-\mu(t)/N$ of the operator $\hat{A} = \hat{B} = \hat{S}^x$. We compare exact quantum ED dynamics for different system sizes $N = 10 \div 18$ (solid lines with increasing color intensity) with TWA results for $N = 16$ (dotted black). An exponential fit of the TWA data with $f(x) = ae^{2\Lambda x}$ yields the exponent $2\Lambda \simeq 1.3/J$. In the left inset we show how the magnetization's dynamics $\langle \hat{S}^x(t) \rangle$ saturates to a finite value $\overline{S^x} \sim 0.1 N$, while on the right the echo saturates to $\overline{\mu} \sim N(\overline{S^x} - \alpha_0) \sim 0.9 N^2$. Dynamics from the fully polarized state along x , with $h = 0.2 J$ over 50 disorder realizations, TWA with $N_{\text{samp}} = 20000$ and $\delta = 0.01$.

References

- [1] L. Boltzmann, *Weitere studien über das wärmegleichgewicht unter gasmolekülen*, In *Kinetische Theorie II*, pp. 115–225. Springer (1970).
- [2] J. Loschmidt, *Sitzungsberichte der akademie der wissenschaften*, Wien, II **73**, 128 (1876).
- [3] W. Thomson, *9. the kinetic theory of the dissipation of energy*, Proceedings of the Royal Society of Edinburgh **8**, 325 (1875).
- [4] A. Peres, *Stability of quantum motion in chaotic and regular systems*, Phys. Rev. A **30**, 1610 (1984), doi:10.1103/PhysRevA.30.1610.
- [5] H. M. Pastawski, P. R. Levstein, G. Usaj, J. Raya and J. Hirschinger, *A nuclear magnetic resonance answer to the boltzmann–loschmidt controversy?*, Physica A: Statistical Mechanics and its Applications **283**(1-2), 166 (2000), doi:10.1016/S0378-4371(00)00146-1.
- [6] P. Jacquod and C. Petitjean, *Decoherence, entanglement and irreversibility in quantum dynamical systems with few degrees of freedom*, Advances in Physics **58**(2), 67 (2009), doi:10.1080/00018730902831009.
- [7] T. Gorin, T. Prosen, T. H. Seligman and M. Žnidarič, *Dynamics of loschmidt echoes and fidelity decay*, Physics Reports **435**(2-5), 33 (2006), doi:10.1016/j.physrep.2006.09.003.
- [8] G. Veble and T. c. v. Prosen, *Classical loschmidt echo in chaotic many-body systems*, Phys. Rev. E **72**, 025202 (2005), doi:10.1103/PhysRevE.72.025202.

- [9] P. R. Levstein, G. Usaj and H. M. Pastawski, *Attenuation of polarization echoes in nuclear magnetic resonance: A study of the emergence of dynamical irreversibility in many-body quantum systems*, The Journal of chemical physics **108**(7), 2718 (1998), doi:10.1063/1.475664.
- [10] B. V. Fine, *Long-time behavior of spin echo*, Phys. Rev. Lett. **94**, 247601 (2005), doi:10.1103/PhysRevLett.94.247601.
- [11] Y. Sekino and L. Susskind, *Fast scramblers*, Journal of High Energy Physics **2008**(10), 065 (2008), doi:10.1088/1126-6708/2008/10/065.
- [12] P. Hosur, X.-L. Qi, D. A. Roberts and B. Yoshida, *Chaos in quantum channels*, Journal of High Energy Physics **2016**(2), 4 (2016), doi:10.1007/JHEP02(2016)004.
- [13] A. Kitaev, *A simple model of quantum holography*, <http://online.kitp.ucsb.edu/online/entangled15/kitaev/> (2015).
- [14] A. Larkin and Y. N. Ovchinnikov, *Quasiclassical method in the theory of superconductivity*, Sov Phys JETP **28**(6), 1200 (1969), doi:10.1016/0378-4371(81)90093-5.
- [15] J. S. Cotler, D. Ding and G. R. Penington, *Out-of-time-order operators and the butterfly effect*, Annals of Physics **396**, 318 (2018), doi:10.1016/j.aop.2018.07.020.
- [16] R. A. Jalabert, I. García-Mata and D. A. Wisniacki, *Semiclassical theory of out-of-time-order correlators for low-dimensional classically chaotic systems*, Phys. Rev. E **98**, 062218 (2018), doi:10.1103/PhysRevE.98.062218.
- [17] S. W. Morgan, V. Oganesyan and G. S. Boutis, *Multispin correlations and pseudothermization of the transient density matrix in solid-state nmr: Free induction decay and magic echo*, Phys. Rev. B **86**, 214410 (2012), doi:10.1103/PhysRevB.86.214410.
- [18] E. G. Sorte, B. V. Fine and B. Saam, *Long-time behavior of nuclear spin decays in various lattices*, Phys. Rev. B **83**, 064302 (2011), doi:10.1103/PhysRevB.83.064302.
- [19] G. Boutis, P. Cappellaro, H. Cho, C. Ramanathan and D. Cory, *Pulse error compensating symmetric magic-echo trains*, Journal of Magnetic Resonance **161**(2), 132 (2003), doi:10.1016/S1090-7807(03)00010-7.
- [20] W.-K. Rhim, A. Pines and J. S. Waugh, *Time-reversal experiments in dipolar-coupled spin systems*, Phys. Rev. B **3**, 684 (1971), doi:10.1103/PhysRevB.3.684.
- [21] B. V. Fine, T. A. Elsayed, C. M. Kropf and A. S. de Wijn, *Absence of exponential sensitivity to small perturbations in nonintegrable systems of spins 1/2*, Phys. Rev. E **89**, 012923 (2014), doi:10.1103/PhysRevE.89.012923.
- [22] T. A. Elsayed and B. V. Fine, *Sensitivity to small perturbations in systems of large quantum spins*, Physica Scripta **2015**(T165), 014011 (2015), doi:10.1088/0031-8949/2015/t165/014011.
- [23] A. E. Tarkhov, S. Wimberger and B. V. Fine, *Extracting lyapunov exponents from the echo dynamics of bose-einstein condensates on a lattice*, Phys. Rev. A **96**, 023624 (2017), doi:10.1103/PhysRevA.96.023624.

- [24] M. Schmitt and S. Kehrein, *Effective time reversal and echo dynamics in the transverse field ising model*, EPL (Europhysics Letters) **115**(5), 50001 (2016), doi:10.1209/0295-5075/115/50001.
- [25] M. Schmitt and S. Kehrein, *Irreversible dynamics in quantum many-body systems*, Phys. Rev. B **98**, 180301 (2018), doi:10.1103/PhysRevB.98.180301.
- [26] M. Schmitt, D. Sels, S. Kehrein and A. Polkovnikov, *Semiclassical echo dynamics in the sachdev-ye-kitaev model*, Physical Review B **99**(13), 134301 (2019), doi:10.1103/PhysRevB.99.134301.
- [27] E. B. Rozenbaum, S. Ganeshan and V. Galitski, *Lyapunov exponent and out-of-time-ordered correlator's growth rate in a chaotic system*, Phys. Rev. Lett. **118**, 086801 (2017), doi:10.1103/PhysRevLett.118.086801.
- [28] S. Pappalardi, A. Russomanno, B. Žunkovič, F. Iemini, A. Silva and R. Fazio, *Scrambling and entanglement spreading in long-range spin chains*, Phys. Rev. B **98**, 134303 (2018), doi:10.1103/PhysRevB.98.134303.
- [29] J. Chávez-Carlos, B. López-del Carpio, M. A. Bastarrachea-Magnani, P. Stránský, S. Lerma-Hernández, L. F. Santos and J. G. Hirsch, *Quantum and classical lyapunov exponents in atom-field interaction systems*, Phys. Rev. Lett. **122**, 024101 (2019), doi:10.1103/PhysRevLett.122.024101.
- [30] R. Lewis-Swan, A. Safavi-Naini, J. Bollinger and A. Rey, *Unifying scrambling, thermalization and entanglement through measurement of fidelity out-of-time-order correlators in the dicke model*, Nature communications **10**(1), 1581 (2019), doi:10.1038/s41467-019-09436-y.
- [31] B. Craps, M. De Clerck, D. Janssens, V. Luyten and R. Charles, *Lyapunov growth in quantum spin chains*, arXiv:1908.08059 (2019).
- [32] T. Scaffidi and E. Altman, *Semiclassical theory of many-body quantum chaos and its bound*, arXiv:1711.04768 (2017).
- [33] I. Kukuljan, S. Grozdanov and T. Prosen, *Weak quantum chaos*, Phys. Rev. B **96**, 060301 (2017), doi:10.1103/PhysRevB.96.060301.
- [34] P. Ray, B. K. Chakrabarti and A. Chakrabarti, *Sherrington-kirkpatrick model in a transverse field: Absence of replica symmetry breaking due to quantum fluctuations*, Phys. Rev. B **39**, 11828 (1989), doi:10.1103/PhysRevB.39.11828.
- [35] J. Miller and D. A. Huse, *Zero-temperature critical behavior of the infinite-range quantum ising spin glass*, Phys. Rev. Lett. **70**, 3147 (1993), doi:10.1103/PhysRevLett.70.3147.
- [36] A. Andreanov and M. Müller, *Long-range quantum ising spin glasses at $t=0$: Gapless collective excitations and universality*, Phys. Rev. Lett. **109**, 177201 (2012), doi:10.1103/PhysRevLett.109.177201.
- [37] N. Y. Yao, F. Grusdt, B. Swingle, M. D. Lukin, D. M. Stamper-Kurn, J. E. Moore and E. A. Demler, *Interferometric approach to probing fast scrambling*, arXiv:1607.01801 (2016).

- [38] M. Hillery, R. F. O’Connell, M. O. Scully and E. P. Wigner, *Distribution functions in physics: fundamentals*, Physics reports **106**(3), 121 (1984), doi:10.1016/0370-1573(84)90160-1.
- [39] M. J. Steel, M. K. Olsen, L. I. Plimak, P. D. Drummond, S. M. Tan, M. J. Collett, D. F. Walls and R. Graham, *Dynamical quantum noise in trapped bose-einstein condensates*, Physical Review A **58**(6), 4824 (1998), doi:10.1103/physreva.58.4824.
- [40] P. Blakie†, A. Bradley†, M. Davis, R. Ballagh and C. Gardiner, *Dynamics and statistical mechanics of ultra-cold bose gases using c-field techniques*, Advances in Physics **57**(5), 363 (2008), doi:10.1080/00018730802564254.
- [41] A. Polkovnikov, *Phase space representation of quantum dynamics*, Annals of Physics **325**(8), 1790 (2010), doi:10.1016/j.aop.2010.02.006.
- [42] E. B. Rozenbaum, S. Ganeshan and V. Galitski, *Universal level statistics of the out-of-time-ordered operator*, arXiv:1801.10591 (2018).
- [43] J. Kurchan, *Quantum bound to chaos and the semiclassical limit*, Journal of Statistical Physics **171**(6), 965 (2018).
- [44] B. Yan, L. Cincio and W. H. Zurek, *Information scrambling and loschmidt echo*, arXiv:1903.02651 (2019).
- [45] M. Srednicki, *The approach to thermal equilibrium in quantized chaotic systems*, Journal of Physics A: Mathematical and General **32**(7), 1163 (1999), doi:10.1088/0305-4470/32/7/007.
- [46] L. D’Alessio, Y. Kafri, A. Polkovnikov and M. Rigol, *From quantum chaos and eigenstate thermalization to statistical mechanics and thermodynamics*, Advances in Physics **65**(3), 239 (2016), doi:10.1080/00018732.2016.1198134.
- [47] C. Murthy and M. Srednicki, *Bounds on chaos from the eigenstate thermalization hypothesis*, arXiv:1906.10808 (2019).
- [48] P. Hosur, X.-L. Qi, D. A. Roberts and B. Yoshida, *Chaos in quantum channels*, Journal of High Energy Physics (2016), doi:10.1007/JHEP02(2016)004.
- [49] D. Sherrington and S. Kirkpatrick, *Solvable model of a spin-glass*, Phys. Rev. Lett. **35**, 1792 (1975), doi:10.1103/PhysRevLett.35.1792.
- [50] G. Parisi, *Infinite number of order parameters for spin-glasses*, Phys. Rev. Lett. **43**, 1754 (1979), doi:10.1103/PhysRevLett.43.1754.
- [51] L. F. Cugliandolo, D. R. Grempel, G. Lozano and H. Lozza, *Effects of dissipation on disordered quantum spin models*, Physical Review B **70**(2) (2004), doi:10.1103/physrevb.70.024422.
- [52] C. Laumann, A. Pal and A. Scardicchio, *Many-body mobility edge in a mean-field quantum spin glass*, Physical Review Letters **113**(20) (2014), doi:10.1103/physrevlett.113.200405.

- [53] C. Baldwin, C. Laumann, A. Pal and A. Scardicchio, *Clustering of nonergodic eigenstates in quantum spin glasses*, Phys. Rev. Lett. **118**(12), 127201 (2017), doi:10.1103/PhysRevLett.118.127201.
- [54] C. L. Baldwin and C. R. Laumann, *Quantum algorithm for energy matching in hard optimization problems*, Physical Review B **97**(22) (2018), doi:10.1103/physrevb.97.224201.
- [55] A. Keleş, E. Zhao and W. V. Liu, *Scrambling dynamics and many-body chaos in a random dipolar spin model*, Physical Review A **99**(5) (2019), doi:10.1103/physreva.99.053620.
- [56] J. Marino and A. M. Rey, *Cavity-QED simulator of slow and fast scrambling*, Physical Review A **99**(5) (2019), doi:10.1103/physreva.99.051803.
- [57] W. K. Wootters, *A wigner-function formulation of finite-state quantum mechanics*, Annals of Physics **176**(1), 1 (1987), doi:10.1016/0003-4916(87)90176-x.
- [58] J. Schachenmayer, A. Pikovski and A. M. Rey, *Many-body quantum spin dynamics with monte carlo trajectories on a discrete phase space*, Phys. Rev. X **5**, 011022 (2015), doi:10.1103/PhysRevX.5.011022.
- [59] T. L. Curtright, D. B. Fairlie and C. K. Zachos, *A concise treatise on quantum mechanics in phase space*, World Scientific Publishing Company, doi:10.1142/5287 (2013).
- [60] J. Wurtz, A. Polkovnikov and D. Sels, *Cluster truncated wigner approximation in strongly interacting systems*, Annals of Physics **395**, 341 (2018), doi:https://doi.org/10.1016/j.aop.2018.06.001.
- [61] I. L. Aleiner and A. I. Larkin, *Divergence of classical trajectories and weak localization*, Phys. Rev. B **54**, 14423 (1996), doi:10.1103/PhysRevB.54.14423.
- [62] R. Schubert, R. O. Vallejos and F. Toscano, *How do wave packets spread? time evolution on ehrenfest time scales*, Journal of Physics A: Mathematical and Theoretical **45**(21), 215307 (2012), doi:10.1088/1751-8113/45/21/215307.
- [63] R. Schubert, R. O. Vallejos and F. Toscano, *How do wave packets spread? time evolution on ehrenfest time scales*, Journal of Physics A: Mathematical and Theoretical **45**(21), 215307 (2012), doi:10.1088/1751-8113/45/21/215307.
- [64] R. B. Sidje, *Expokit: A software package for computing matrix exponentials*, ACM Transactions on Mathematical Software (TOMS) **24**(1), 130 (1998), doi:10.1145/285861.285868.
- [65] H. Fujisaka, *Statistical dynamics generated by fluctuations of local lyapunov exponents*, Progress of theoretical physics **70**(5), 1264 (1983), doi:10.1143/PTP.70.1264.
- [66] R. Benzi, G. Paladin, G. Parisi and A. Vulpiani, *Characterisation of intermittency in chaotic systems*, Journal of Physics A: Mathematical and General **18**(12), 2157 (1985).
- [67] A. E. Tarkhov and B. V. Fine, *Estimating ergodization time of a chaotic many-particle system from a time reversal of equilibrium noise*, New Journal of Physics **20**(12), 123021 (2018), doi:10.1088/1367-2630/aaf0b6.